MEMS Electrostatic Acoustic Pixel

Arpys Arevalo[*1], David Conchouso[1], David Castro[1], and Ian G. Foulds[1,3]
[1]Computer, Electrical and Mathematical Sciences and Engineering (CEMSE), King Abdullah University of Science and Technology (KAUST), [2]The University of British Columbia (UBC), School of Engineering, Okanagan Campus.
*Corresponding author: 4700 KAUST, Kingdom of Saudi Arabia, arpys.arevalo@kaust.edu.sa

Abstract: This paper reports the simulation of an hexagonal membrane structure using COMSOL Multiphysics 5.0. The structure is a $5\mu m$ thick polyimide layer with an integrated metal layer on top, to apply a bias voltage. The hexagonal membrane is separated by a $3\mu m$ air gap and $5\mu m$ thick polyimide structural layer from the bottom electrode and a $3\mu m$ and $5\mu m$ thick polyimide structural layer from the top electrode. The AC/DC Module was used to extract the capacitance and pull-in voltage needed to displace the membrane toward the active electrode. A modal analysis was performed using the Structural Mechanics Module to extract the structure's resonance frequency and frequency modes.

Keywords: MEMS, electrostatic speaker, digital sound reconstruction, Acoustic Pixel, polyimide.

1. Introduction

The growth of the electronics industry demands better components for improved electronic systems [1, 2]. Such components need to be more advanced in order to keep up with the evolution of the digital era. The loudspeaker design mechanism has not been changed for almost a century [3–5]. In an era were almost every component is digital, the loudspeaker driver design still is the last analog component that needs to evolve to its digital form, to achieve a true digital audio reproduction cycle.

Efforts to develop a direct digital method of sound reconstruction has been reported elsewhere [6, 7]. In [4], authors reported a micro-speaker in a single chip using CMOS-MEMS membrane arrays and described their method behind the digital sound reconstruction concept. They fabricated a 3-bit electrostatic array (seven transducer element) where they demonstrated the sound reconstruction. Due to their fabrication methods each transducer in the array has a fixed electrode with a dome shape membrane. Therefore, there is an asymmetry in their system while actuating the membranes.

In previous work, we have tackled this problem by using a piezoelectric layer [7–9]. Using the latter method for the driving mechanism help us to avoid the asymmetry in the system, but adds some complexity to the fabrication process. Our work differs from other reports [10–14], specifically in the dimensions of the actuator, the combination of materials used, the micro fabrications process and the method of sound reconstruction.

In this work we propose an electrostatic approach using Polyimide as the structural layer. Polyimide is a very attractive polymer for MEMS fabrication due to its low coefficient of thermal expansion, low film stress, lower cost than metals and semiconductors and high temperature stability compared to other polymers [15–17]. Polyimide has been previously used in the microelectronics industry for module packaging, flexible circuits and as a dielectric for multi-level interconnection technology [18, 19]. Polyimide has demonstrated great performance in Micro Electro Mechanical Systems (MEMS) devices [15, 20–34] and in the microelectronics industry. The polymer can handle temperatures of up to 350°C and can be easily processed and integrated with metal layers to develop devices with low complexity.

2. Computational Methods

COMSOL Multiphysics provides the Electrostatic Interface, which is available for 3D, 2D in-plane and 2D axisymmetric components. In our particular application we have a capacitor which will use relatively high voltage (up to 150 Volts).

The electrostatic equations are not to be taken literally as "statics", but as the observation or time scale at which the applied excitation changes are in comparison to the charge relaxation time, and that the electromagnetic wavelength and skin depth are very large compared to the size of the domain of interest [35].

For our device, we need to use the quasi-static electric fields and currents that are included in the MEMS module, together with the AC/DC Module, which do not include the wave propagation effects. The physics interfaces takes only the scalar electric potential, which can be interpreted in terms of the charge relaxation process. The three equations used for this physic are: The Ohm's Law, the equation of continuity and the Gauss' law. COMSOL combines this equation and uses the following differential equation for the space charge density in a homogeneous medium:

$$\frac{\delta\rho}{\delta t} + \frac{\sigma}{\varepsilon}\rho = 0 \tag{1}$$

with solution:

$$\rho(t) = \rho_0 e^{\frac{-t}{\tau}} \tag{2}$$

where

$$\tau = \frac{\varepsilon}{\sigma} \tag{3}$$

which is the charge relaxation time. When using a good conductor material such as gold, τ is of the order of $10^{-}19$s whereas for a good insulator like silicon oxide, its of the order of 10^3s. It is the relation between the external time scale and the charge relaxation time that determines the physics interface and study that we will use.

2.1 Electrostatic Equations

Under static condition the potential, V, is defined as the following relationship:

$$E = -\nabla V \tag{4}$$

When combined with the constitutive relationship $D = \varepsilon E + P$ bettwen the electric displacement D and the electric field E, the Gauss' law is represented as:

$$-\nabla \cdot (\varepsilon_0 \nabla V - P) = \rho \tag{5}$$

The equation describes the electrostatic field in dielectric materials, the physical constant ε_0 is the permittivity of vacuum with units $[F/m]$, P is the electric polarization vector in $[C/m^2]$, and ρ is the space charge density given in $[C/m^3]$.

For models in 2D, the interface assumes a symmetry where the electric potential varies only in the x and y directions and is constant in the z direction. Which implies that the electric field E is tangential to the xy-plane. The same equation is solved in the case of a 3D model. The interface sovles the following equation where d is the thicness int eh z direction:

$$-\nabla \cdot (\varepsilon_0 \nabla V - P) = \rho \tag{6}$$

The axisymmetric version of the physics interface considers the situation where the fields and geometry are axially symmetric. For this case the electric potential is constant in the ϕ direction, implying that the electric field is tangential to the rz-plane [35].

3. Design and Simulation Setup

The main membrane of our device can be divided in three sections: outer hexagonal ring, tethers and hexagonal membrane (see Fig. 1).

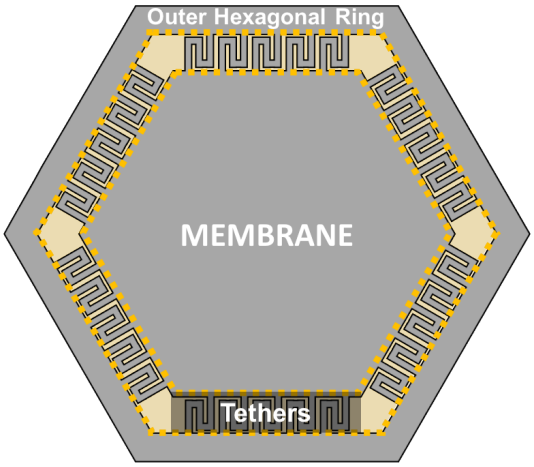

Figure 1: Top view of the simulated membrane, showing its three different sections.

The device was evaluated with several different tether designs and the present work is done using the final chosen design for fabrication. The design shows 5 tethers in each side of the hexagonal

membrane. The standard structure has the following dimensions: 250μm membrane hexagon side, the hexagon was inscribed in a 500μm diameter circumference and tether have a width of 8μm for each of them.

The structure can be fabricated using two structural layers and two sacrificial layers. The structural layers are made of polyimide and have a thickness of 5μm. To be able to attract and repel the membrane we need a set of electrodes. In our simulations we use the bottom electrode made of gold, because of its good conductivity, which is located right on the silicon substrate. Also a middle electrode which is on top of the membrane and a top electrode that is all the way to the top of the structure. Fig. 2 shows a conceptual view of an individual membrane.

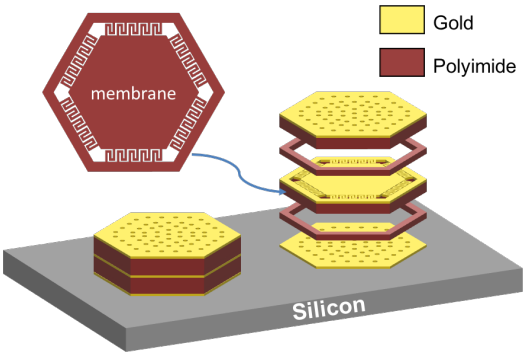

Figure 2: Conceptual view of the simulated device. The image shows an exploded view on the right, and an assembled view on the left.

To create the 3D model in COMSOL, we first exported the 2D layout from Tanner L-edit software, which is the tool we use to design our devices for micro-fabrication. The CAD import module was used, and the correct scale was set to import the DXF file into COMSOL environment. The import was done in two different work-planes to be able to extrude the needed features. The final component was set to form composite faces to eliminate unnecessary features and a union operation.

The selected materials for the electrodes was gold, as depicted in Fig. 2 in yellow color. The structural layer was set to be polyimide, shown in red color in Fig. 2. Also, all the gaps were set to be air. Table 1 contains the material properties used in the simulation.

Table 1: Materials Properties

Property	**Polyimide**	**Gold**
Relative permittivity (ε_r)	2.9	6.9
Young's modulus (E)	$3.1e^9\,[Pa]$	$70e^9\,[Pa]$
Poisson's ratio (ν)	0.34	0.44
Density (ρ)	$1300\,[kg/m^3]$	$19300[kg/m^3]$

The Electromechanics physics module was setup with the following constraints: Fixed constraint for all the six outer sides (faces boundaries) of the full structure, Bottom Electrode as the ground and Middle Electrode as a Terminal. The setup will allow the interaction between the electrodes, and the capacitance will be calculated by the software.

An interesting feature of our design is that there will not be an electric short when pull-in occurs, because all the electrodes are completely isolated from each other with structural layer.

To see the behavior of the membrane we used a Stationary Study with an auxiliary sweep to apply voltages between a pair of electrodes ranging from 10V - 150V in steps of 10V. The boundary that was set to be a terminal was given the declared parameter "Vin".

4. Results

The simulation results give us an insight of the deformation of the membrane. It is known that the pull-in voltage when the system is unstable, which happens at approximately $1/3$ of the distance between the electrodes. Therefore, the pull-in will occur when the membrane moves approximately 2.6μm towards the active electrode. In Fig. 3 a graph of the simulated displacement vs the applied voltage is shown. Fig. 5 shows the graph of the capacitance between the electrodes vs the applied voltage.

From these results we were able to deduct that the pull-in voltage is between 140V and 150V, applying more than this voltage wont let the simulation to converge. Fig. shows the result of the displacement in the 3D model.

The resonance frequency and mode frequencies were calculated using the Solid Mechanics Module to study the behavior of the structure. An

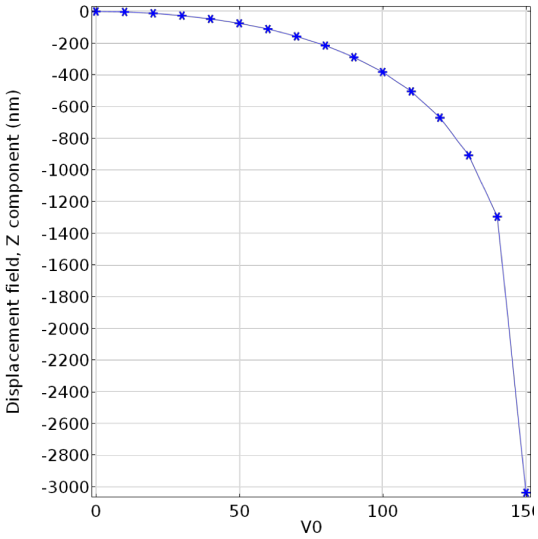

Figure 3: Total displacement on the "z-axis" vs the applied voltage.

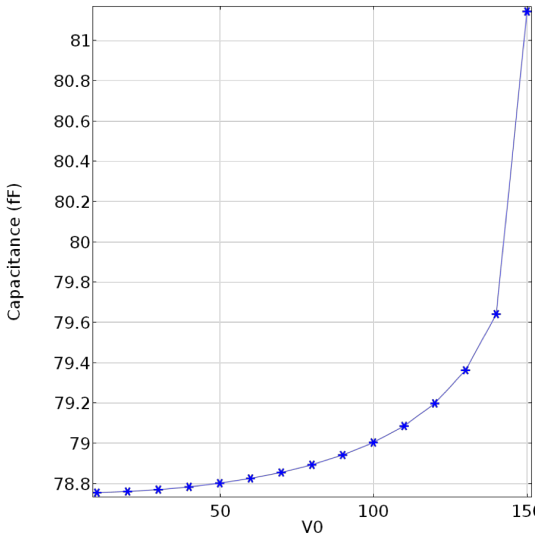

Figure 4: Capacitance vs applied voltage.

Eigenfrequency study was setup to find the first 6 modes of the structure, shown in Fig. 6.

From this simulation we can see that the mode of interest is the first one at $9.4175\,kHz$, as this will displace the air in a uniform mode with only one deformation node. Since the transducer will be actuated at an expected sample frequency of $40\,kHz$, the closest mode is the sixth at $3.9267\,kHaz$. Mode 6, has one radial node and one central node, but it will not have an impact in the performance of the membrane because it will be out of the range of the frequency.

If the membrane will be actuated at $40\,kHz$, this means that the input signal will behave as a pulse with a width of $25\,\mu m$. Therefore, we performed a new simulation with at Time Dependent Study from $t = 0$ to $t = 625\,\mu s$ in steps of $25\,\mu s$ to observe the response time of the structure to a $150\,V$ constant electric potential applied to one of the electrode. Fig. 7, shows the response time of the membrane. From this graph we can see that it takes the membrane approximately $125\,\mu s$ to reach the maximum displacement of about $1.5\,\mu m$. Also, it can be seen that it the membrane reaches a stable position in approximately $500\,\mu s$ at $1\,\mu m$ displacement from its original position. Nevertheless, the pulses will only be $25\,\mu s$ long and this means that the structure will only displace approximately $0.5\,\mu m$.

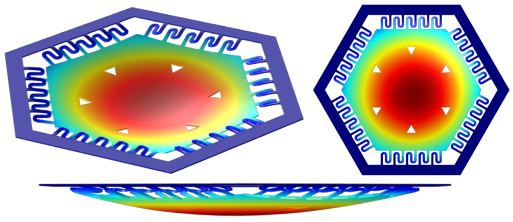

Figure 5: (Top Left) Isometric view of the simulation results for displacement, (Top Right) Top view of deformed structure, (Bottom) Side view of the deformed structure at 150V.

5. Conclusions

The proposed membrane design was simulated with the intended operation voltages for the real device. The results shows that the membrane is suitable for the intended acoustic transducer element for the final transducer array. The membrane geometry can be adjusted to change the structure resonance frequency, so that the element has the optimal acoustic response. The next simulation steps will be the acoustic response. Now that we have found the total displacement of the structure at an applied voltage, we can simulate the displacement and calculate the sound pressure generated by this change.

Full arrays have already been designed and fabricated. The processed chips are diced from a four inch wafer using our in house dicing method [36].

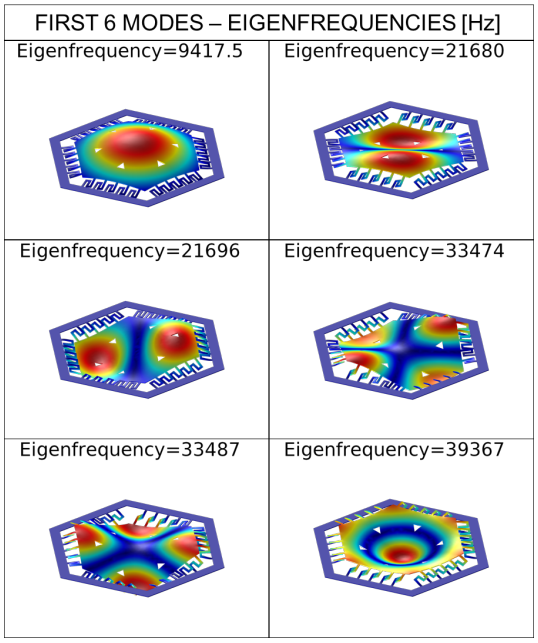

Figure 6: Frequency modes of the simulated structures

The chips are currently being tested and the next steps include the validation of the presented model and the experimental results.

6. References

1. J P Rojas, A Arevalo, I G Foulds, and M M Hussain. Design and characterization of ultra-stretchable monolithic silicon fabric. *Applied Physics Letters*, **105**(15):154101, (2014).

2. J P Rojas, Hussain A M, A Arevalo, I G Foulds, Sevilla GAT, JM Nassar, and M M Hussain. Transformational electronics are now reconfiguring. *SPIE Defense+ Security*, **9467**:946709–946709–7, (2015).

3. Carl B Boyer and Uta C Merzbach. *A History of Mathematics*. Wiley (2011).

4. Brett M Diamond, John J Neumann, Jr, and Kaigham J Gabriel. Digital sound reconstruction using arrays of CMOS-MEMS microspeakers. In *Micro Electro Mechanical Systems, 2002. The Fifteenth IEEE International Conference on*, pages 292–295, (2002).

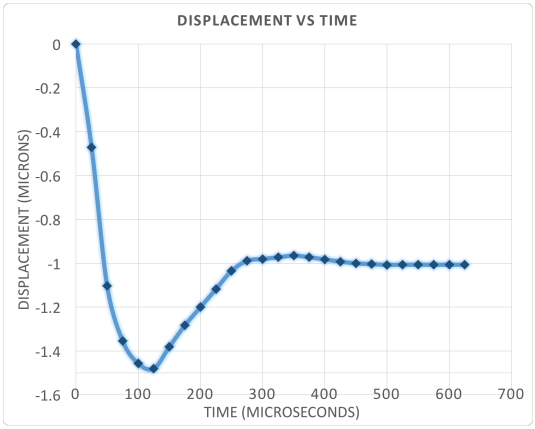

Figure 7: Response time of the structure to an input signal of $150V$

5. Baron John William Strutt Rayleigh and Robert Bruce Lindsay. *The theory of sound* (1945).

6. B.M Diamond, J.J. Jr Neumann, and K.J Gabriel. Digital sound reconstruction using arrays of CMOS-MEMS microspeakers. In *Micro Electro Mechanical Systems, 2002. The Fifteenth IEEE International Conference on*, pages 292–295, (2002).

7. A Arevalo, D Conchouso, D Castro, N Jaber, M I Younis, and I G Foulds. Towards a Digital Sound Reconstruction MEMS Device: Characterization of a Single PZT Based Piezoelectric Actuator. In *10th IEEE International Conference on Nano/Micro Engineered and Molecular Systems NEMS2015*, Xia'an (2015).

8. A Arevalo and I G Foulds. MEMS Acoustic Pixel. *2014 COMSOL Conference, Cambridge, England*, (2014).

9. A Arevalo and I G Foulds. Parametric Study of Polyimide-Lead Zirconate Titanate Thin Film Cantilevers for Transducer Applications. In *2013 COMSOL Conference, Rotterdam, Holland*, (2013).

10. Zhihong Wang, Jianmin Miao, and Chee Wee Tan. Acoustic transducers with a perforated damping backplate based on PZT/silicon wafer bonding technique. *Sensors and Actuators A: Physical*, **149**(2):277–283 (2009).

11. Youngki Choe, S Chen, and Eun Sok Kim. High fidelity loud microspeaker based on PZT bimorph diaphragm. In *NSTI-Nanotech 2010*, pages 316–319, (2010).

12. Sang-Soo Je and Junseok Chae. A Compact, Low-Power, and Electromagnetically Actuated Microspeaker for Hearing Aids. *Electron Device Letters, IEEE*, **29**(8):856–858, (2008).

13. P Valousek. A digital loudspeaker: experimental construction. *Acta polytechnica*, **46**:40–42, (2006).

14. Nicolas-Alexander Tatlas and John N Mourjopoulos. Digital Loudspeaker Arrays driven by 1-bit signals. In *Audio Engineering Society Convention 116*, (2004).

15. A Arevalo, E Byas, D Conchouso, D Castro, S Ilyas, and I G Foulds. A Versatile Multi-User Polyimide Surface Micromachining Process for MEMS Applications. In *10th IEEE International Conference on Nano/Micro Engineered and Molecular Systems NEMS2015*, Xia'an (2015).

16. A A A Carreno, D Conchouso, A Zaher, I Foulds, and J Kosel. Simulation of a Low Frequency Z-Axis SU-8 Accelerometer in CoventorWare and MEMS+. In *Computer Modelling and Simulation (UKSim), 2013 UKSim 15th International Conference on*, pages 792–797, (2013).

17. D Conchouso, A Arevalo, D Castro, E Rawashdeh, M Valencia, A Zaher, J Kosel, and I Foulds. Simulation of SU-8 Frequency-Driven Scratch Drive Actuators. In *Computer Modelling and Simulation (UKSim), 2013 UKSim 15th International Conference on*, pages 803–808, (2013).

18. A Bruno Frazier. Recent applications of polyimide to micromachining technology. *Industrial Electronics, IEEE Transactions on*, **42**(5):442–448, (1995).

19. A B Frazier. Uses of polyimide for micromachining applications. In *Industrial Electronics, Control and Instrumentation, 1994. IECON '94., 20th International Conference on*, pages 1483–1487, (1994).

20. S.Y. Xiao, L.F. Che, X.X. Li, and Y.L. Wang. A novel fabrication process of {MEMS} devices on polyimide flexible substrates. *Microelectronic Engineering*, **85**(2):452 – 457, (2008).

21. Steve Tung, Scott R Witherspoon, Larry A Roe, Al Silano, David P Maynard, and Ned Ferraro. A mems-based flexible sensor and actuator system for space inflatable structures. *Smart Materials and Structures*, **10**(6):1230, (2001).

22. J. Courbat, M.D. Canonica, D. Briand, N.F. de Rooij, Damien Teyssieux, Laurent Thiery, and Bernard Cretin. Thermal simulation and characterization for the design of ultra-low power micro-hotplates on flexible substrate. In *Sensors, 2008 IEEE*, pages 74–77 (2008).

23. A Arevalo, E Byas, and I G Foulds. μHeater on a Buckled Cantilever Plate for Gas Sensor Applications. *2012 COMSOL Conference, Milan, Italy*, (2012).

24. A Arevalo, D Conchouso, and I G Fould. Optimized Cantilever-to-Anchor Configuration of Buckled Cantilever Plate Structures for Transducer Applications. *2012 COMSOL Conference, Milan, Italy*, (2012).

25. A Arevalo, S Ilyas, D Conchouso, and I G Foulds. Simulation of a Polyimide Based Micromirror. *2014 COMSOL Conference*, (2014).

26. A Arevalo and I G Foulds. Polyimide Thermal Micro Actuator. *2014 COMSOL Conference, Cambridge, England*, (2014).

27. S Ilyas, A Ramini, A Arevalo, and M I Younis. An Experimental and Theoretical Investigation of a Micromirror Under Mixed-Frequency Excitation. *Journal of Microelectromechanical Systems*, (2015).

28. D Conchouso, A Arevalo, D Castro, , and I G Foulds. Out-of-plane Platforms with Bi-directional Thermal Bimorph Actuation for Transducer Applications. In *10th IEEE International Conference on Nano/Micro Engineered and Molecular Systems NEMS2015*, Xia'an (2015).

29. Loïc Marnat, A Arevalo Carreno, D Conchouso, M Galicia Martinez, I Foulds, and Atif Shamim. New Movable Plate for Efficient Millimeter Wave Vertical on-Chip Antenna. *IEEE Transactions on Antennas and Propagation*, **61**(4):1608–1615, (2013).

30. A Alfadhel and Arpys Arevalo. Three-Axis Magnetic Field Induction Sensor Realized on Buckled Cantilever Plate. ... *IEEE Transactions on*, (2013).

31. D Castro, A Arevalo, E Rawashdeh, and N Dechev. Simulation of a Micro-Scale Out-of-plane Compliant Mechanism. In *2014 COMSOL Cambridge, England*, (2014).

32. A Arevalo, D Conchouso, D Castro, M Diaz, and I G Foulds. Out-of-plane buckled cantilever microstructures with adjustable angular positions using thermal bimorph actuation for transducer applications. *Micro and Nano Letters*, (2015).

33. A Arevalo, D Conchouso, E Rawashdeh, D Castro, and I G fould. Platform Isolation Using Out-of-Plane Compliant Mechanisms. In *2014 COMSOL Conference, Boston, USA* (2014).

34. N Jaber, A Ramini, A Carreno, and MI Younis. Higher Order Modes Excitation of Micro Clamped-Clamped Beams. *NANOTECH Dubai 2015*, (2015).

35. COMOSL. Comsol multiphysics reference manual. (2015).

36. Y Fan, A Arevalo, H Li, and I G Foulds. Low-cost silicon wafer dicing using a craft cutter. *Microsystem Technologies*, (2014).